REPORT DOCUMENTATION PAGE

Form Approved
OMB NO. 0704-0188

1. AGENCY USE ONLY (Leave Blank)	2. REPORT DATE	3. REPORT TYPE AND DATES COVERED
	28 Sept 04	**Final Progress Report, 01 Jul 00 – 30 Jun 04**

4. TITLE AND SUBTITLE
Self-Assembled Materials Systems and Devices for R-FLICS

5. FUNDING NUMBERS
DAAD19-00-1-0368

6. AUTHOR(S)
Seng-Tiong Ho & Tobin J. Marks

7. PERFORMING ORGANIZATION NAME(S) AND ADDRESS(ES)
Department of Electrical and Computer Engineering / Department of Chemistry
Northwestern University, 2145 Sheridan Rd., Evanston, IL 60208

8. PERFORMING ORGANIZATION REPORT NUMBER

9. SPONSORING / MONITORING AGENCY NAME(S) AND ADDRESS(ES)

U. S. Army Research Office
P.O. Box 12211
Research Triangle Park, NC 27709-2211

10. SPONSORING / MONITORING AGENCY REPORT NUMBER

41315.23-EL-DRP

11. SUPPLEMENTARY NOTES
The views, opinions and/or findings contained in this report are those of the author(s) and should not be construed as an official Department of the Army position, policy or decision, unless so designated by other documentation.

12 a. DISTRIBUTION / AVAILABILITY STATEMENT

Approved for public release; distribution unlimited.

12 b. DISTRIBUTION CODE

13. ABSTRACT (Maximum 200 words)

Electro-optic (EO) modulators based on multilayer self-assembled superlattices (SAS) from wet deposition, and from vapor phase deposition have been designed, fabricated, and characterized. Two-step wet chemical protection-deprotection approach for the growth of SAS was used for the fabrication of electro-optic modulators. With this process the SAS film can be grown at a rate of about 40 minutes per bilayer, and it is at least one order of magnitude more rapid than previous three-step deposition method. Novel approaches of self-assembly via vapor phase deposition were investigated for the growth of EO active DTPT, and PEPCOOH thin films. The EO active thin films exhibit strong second harmonic generation and EO modulation effects without external electric field poling. Promising electro-optic materials were used for the grown of EO thin films from vapor phase, and prototype electro-optic modulators were fabricated and tested by integrating the intrinsically acentric self-assembled thin films with low-loss polymeric layers and semiconductor substrates.

14. SUBJECT TERMS	15. NUMBER OF PAGES
electro-optic modulator, self-assembly, organic electro-optic material, modulator, and RFLICS.	30
	16. PRICE CODE

17. SECURITY CLASSIFICATION OR REPORT	18. SECURITY CLASSIFICATION ON THIS PAGE	19. SECURITY CLASSIFICATION OF ABSTRACT	20. LIMITATION OF ABSTRACT
UNCLASSIFIED	**UNCLASSIFIED**	**UNCLASSIFIED**	**UL**

NSN 7540-01-280-5500

Standard Form 298 (Rev.2-89)
Prescribed by ANSI Std. 239-18
298-102

REPORT DOCUMENTATION PAGE (SF298)
(Continuation Sheet)

Table of Contents

(1) List of Appendixes, Illustrations and Tables

See Table of Contents, Page I.

(2) Statement of the problem studied

The implementation of RF Photonics systems require the realization of electro-optic (EO) modulators that can provide low switching voltages. The current EO modulators based on $LiNbO_3$ have reached their performance limits in terms of switching voltages. The main goals of this project is to realize EO modulators based on self-assembled superlattice (SAS) organic polymers, which will solve the problems facing current poled-polymers organic modulators in terms of manufacturability.

(3) Summary of the most important results

1. Achieved expeditious, two-step growth of robust, structurally regular, acentric SAS.
2. No external electric field poling needed for the achievement of nonlinearity of SAS thin films.
3. Automated growth apparatus implemented for SAS structures.
4. Metal oxide layer incorporation demonstrated for index tuning of SAS thin films.
5. Introduction of high-response chromophores into SAS structures.
6. Introduction of fast vapor phase deposition methods for the growth of EO active thin films.
7. Demonstrated long-term stability, thermal stability, and irradiation stability of SAS thin films.
8. All polymer waveguides demonstrated good transparencies (0.5 dB/cm) from 350nm to 1650nm covering OFC wavelengths.
9. Fabrication and characterization of prototype EO modulators using three-step and novel expeditious two-step grown SAS.
10. Fabrication and characterization of prototype EO modulators using vapor phase deposited EO active thin films of DTPT and PEPCOOH.
11. Different waveguide structures for low loss, strong mode confinement, integration with semiconductor substrates and industrial techniques.

(4) List of papers submitted or published under ARO sponsorship during this reporting period. List the papers, including journal references, in the following categories:

(a) Papers published in peer-reviewed journals

"Polymer Waveguides Useful over a Very Wide Wavelength Range from the Ultraviolet to Infrared", Y. –G. Zhao, W. –K. Lu, Y. Ma, S. –S. Kim, S. T. Ho, and T. J. Marks, *Appl. Phys. Lett*., **77** (19), 2961-2963. (2000).

"Single Reactor Route to Polar Superlattices. Layer-by-Layer Self-Assembly of Large-Response Molecular Electro-Optic Materials by Protection-Deprotection" van der Boom, Milko E.; Richter, Andrew G.; Malinsky, Joshua E.; Lee, P. A.; Armstrong, Neal R.; Dutta, Pulak; Marks, Tobin J. *Chem. of Mater.,* **13**(1), 15-17. (2001).

"Traveling wave electro-optic phase modulators based on intrinsically polar self-assembled chromophoric superlattices", Y. G. Zhao, A. Wu, H.-L. Lu, S. Chang, W.-K. Lu, and S. T. Ho, *Appl. Phys. Lett.*, **79**(5), 587-589, (2001).

Facchetti, A.; van der Boom, M.E.; Abbotto, A.; Beverina, L.; Marks, T.J.; Pagani, G.A. Design and Preparation of Zwitterionic Organic Thin Films: Self-Assembled Siloxane-Based, Thiophene-Spaced *N*-Benzylpyridinium Dicyanomethanides as Nonlinear Optical Materials, *Langmuir*, *17*, 5939-5942. (2001).

van der Boom, M.E.; Evmenenko, G.; Dutta, P.; Marks, T.J. Nanoscale Refractive Index Tuning of Siloxane-Based Self-Assembled Electro-Optic Superlattices, *Advanced Functional Materials*, *11*, 393-397. (2001).

Evmenenko, G.; Dugan, S.W.; Kmetko, J.; Dutta, P.; van der Boom, M.E.; Marks, T.J. Specular X-Ray Reflectivity Study of Ordering in Self-Assembled Organic-Inorganic Electro-Optic Multilayer Films, *J. Chem. Phys.*, *115*, 6722-6727. (2001).

P. Zhu, M. E. van der Boom, H. Kang, G. Evmenenko, P. Dutta, T. J. Marks, "Realization of Expeditious Layer-by-Layer Siloxane-Based Self-Assembly as an Efficient Route to Structurally Regular Acentric Superlattices with Large Electro-Optic Responses," *Chem. Mater.* **14**, 4982-4989. (2002).

van der Boom, M.E.; Zhu, P.; Evmenenko, G.; Malinsky, J.E.; Lin, W.; Dutta, P.; Marks, T.J. Nanoscale Consecutive Self-Assembly of Thin-Film Molecular Materials for Electrooptic Switching. Chemical Streamlining and Ultrahigh Response Chromophores, *Langmuir*, *18*, 3704-3707. (2002).

Wang, G.; Zhu, P.; Marks, T.J.; Ketterson, J.B. Ultra-Fast Frequency-Selective Optical Switching Based on Thin Self-Assembled Organic Chromophoric Films with a Large Second-Order Nonlinear Response," Appl. Phys. Lett., **81**(12), 2169-2171. (2002).

"Waveguide electro-optic modulators based on organic self-assembled superlattices (SASs)", Z. Liu, S. T. Ho, S. S. Chang, and T. J. Marks, *Trends in Optics and Phonics (TOPS)*, (ISBN: 1-55752-705-9), Washington DC, CTuK5. (2002).

Zhao, Y.-G.; Chang, S.; Wu, A.; Lu, H.-L.; Ho, S.T.; van der Boom, M.E.; Marks, T.J. "Second-Generation Approach to All-Organic Modulators Based on Intrinsically Polar Self-Assembled Molecular Superlattices," *Opt. Eng.* **42**(2) 298–299. (2003).

Zhifu Liu, De-Gui Sun, Jing Ma, Yegao Xiao, Seng-Tiong Ho, Hu Kang, Peiwang Zhu, and Tobin Marks, "Self-assembled superlattice thin film waveguide electro-optic phase modulators," *Trends in Optics and Phonics (TOPS)*, (ISBN: 1-55752-733-4), Washington DC, CTuS2. (2003).

Peiwang Zhu, Hu Kang, Antonio Facchetti, Guennadi Evmenenko, Pulak Dutta, and Tobin J. Marks, "Vapor Phase Self-Assembly of Electrooptic Thin Films via Triple Hydrogen Bonds," *J. Am. Chem. Soc.*, **125**(38), 11496-11497. (2003).

Facchetti, A.; Abbotto, A.; Beverina, L.; van der Boom, M. E.; Dutta, P.; Evmenenko, G.; Pagani, G. A.; Marks, T. J.; "Layer-by-Layer Self-Assembled Pyrrole-Based Donor-Acceptor Chromophores as Electro-Optic Materials,**"** *Chem. Mater.,* **15**(5); 1064-1072. (2003).

(b) Papers published in non-peer-reviewed journals or in conference proceedings

"Layer-by-Layer Self-assembly of Large Response Molecular Electro-Optic Materials by a Desilylation Strategy", van der Boom, Milko E.; Richter, Andrew G.; Malinsky, Joshua E.; Dutta, Pulak; Marks, Tobin J.; Lee, P. A.; Armstrong, Neal R., *Polym. Mater. Sci. Eng.* **83,** 160-161, (2000). Reprint not available.

Pagani, G.A.; Marks, T.J.; Abbotto, A.; Beverina, L.; van der Boom, M.E.; Bradamante, S.; Facchetti, A. Novel Heterocycle-Based Dyes for Photonics: Effect of Self-Assembling, Pyridine Annulation, and Medium on Molecular Response, *Polymer Preprints*, *42(2)*, 567-568. (2001). Reprint not available.

Zhu, P.; van der Boom, M.E.; Evmenenko, G.; Dutta, P.; Marks, T.J. Efficient Consecutive Assembly of Large-Response Thin-Film Molecular Electro-Optic Materials, *Polymer Preprints*, *42(2)*, 579-580. (2001).

van der Boom, M.E.; Malinsky, J.E.; Zhao, Y.-G.; Chang, S.; Lu, W.-K.; Ho, S.-T.; Marks, T.J. High-Response Electro-Optic Phase Modulator Based on an Intrinsically Acentric Layer-By-Layer Self-Assembled Molecular Superlattice, *Polymer Preprints*, *42(2),* 550-551. (2001). Reprint not available.

"Waveguide electro-optic modulators based on intrinsically polar self-assembled superlattices (SASs)", (Invited) Zhifu Liu, Seng Tiong Ho , Seongsik Chang , Yiguang Zhao , Tobin J. Marks , Hu Kang, and Peiwang Zhu, SPIE Proc. 4798, pp. 151-162. (2002).

De-Gui Sun, Zhifu Liu, Jing Ma, Yegao Xiao, Seng-Tiong Ho, Hu Kang, Peiwang Zhu, and Tobin Marks, "Loss Minimizing Strategies for Self-Assembled Superlattice Waveguiding Electro-Optic Modulators," in Signals Processing and Optical Systems, Technologies and Applications, Eds. N. Callaos, W. Lesso, El-S. A. El-Badawy, and S. Lachowicz, Proc. Vol. X, *The 7th World Multiconference on Systemics, Cybernetics and Informatics*, pp. 76-80. (2003).

Tobin J. Marks, Seng-Tiong Ho, Zhifu Liu, Peiwang Zhu, De-Gui Sun, Jing Ma, Yegao Xiao, and Hu Kang, "Electro-optic waveguide modulators by the integration of self-assembled superlattice with polymer and semiconductor materials (Invited paper)," in *Organic Photonic Materials and Devices VI*, Eds. James G. Grote, Toshikuni Kaino, Proc. *SPIE* 4991, pp. 133-143. (2003).

Peiwang Zhu; Hu Kang; Antonio Facchetti; Guennadi Evmenenko; Pulak Dutta; and Tobin J. Marks. "Electro-Optic Thin Films Self-Assembled via Multiple Hydrogen Bonds From the Vapor Phase," *Polymeric Materials: Science & Engineering*, **89**, 265-266. (2003).

Hu Kang; Peiwang Zhu; Yu Yang; Guennadi Evmenenko, Pulak Dutta, and Tobin J. Marks, "Self-Assembled Electro-Optic Thin Films with Dramatically Blue-Shifted Optical Absorption Based on Novel X-Shaped Two-Dimensional Charge-Transfer Chromophores", *Polymeric Materials: Science & Engineering*, 91, 267-268. (2004).

(c) Manuscripts submitted, but not published

Facchetti, A.; Annoni, E.; Beverina, L.; Morone, M.; Zhu, P.; Marks, T. J.; Pagani, G. A. "Very Large Electro-Optic Responses in H-Bonded Heteroaromatic Films Grown by Physical Vapor Deposition" *Nature Mater.* IN PRESS.

Seng-Tiong Ho, Zhifu Liu, Jing Ma, Guoyang Xu, Bo Liu, Tobin J. Marks, Peiwang Zhu, Hu Kang, and Antonio Facchetti, "Self-Assembled Materials Systems and Devices for R-FLICS," GOMAC 2004 Conference.

Peiwang Zhu, Hu Kang, Milko E. van der Boom, Zhifu Liu, Guoyang Xu, Jing Ma, Delai Zhou, and Seng-Tiong Ho, Tobin J. Marks, "Self-assembled materials and devices that process light (Invited paper)," SPIE 2004 Meeting (2004).

Hu Kang, Peiwang Zhu, Yu Yang, Antonio Facchetti, and Tobin J. Marks, "Self-Assembled Electro-Optic Thin Films with Remarkably Blue-Shifted Optical Absorption Based on an X-Shaped Chromophore", J. Am. Chem. Soc., submitted

(5) List of all participating scientific personnel showing any advanced degrees earned by them while employed on the project

N/A

(6) Report of inventions (by title only)

"High Response Modulator Based on an Intrinsically Acentric, Layer-by-Layer Self-Assembled Molecular Superlattice"

"Layer-by-Layer Self-Assembly of Large Response Molecular Electro-Optic Materials by a Desilylation Strategy"

"Low loss broad band organic optical waveguide"

"Refractive Index Tuning of Siloxane-Based Electro-Optic Self-Assembled Superlattices"

"Vapor Deposited Electro-optic Films Self-assembled through Hydrogen Bonding"

(7) Bibliography

(In the order of the beginning dates that the persons participated in the project)

Department of Electrical and Computer Engineering, Northwestern University

Prof. Seng-Tiong Ho received his Ph.D. specialized in Electrical Engineering from MIT in March 1989. His research interest is in the areas of microcavity lasers, quantum phenomena in low-dimensional photonic structures, nanofabrication, ultrafast nonlinear optical studies, optical communications, and quantum optics.

Dr. Seongsik Chang, Ph.D. (Yale University). Bibliography not available at time of submission

Dr. Yi-Guang Zhao, Ph.D. (Peking University). Bibliography not available at time of submission

Dr. Zhifu Liu received his Ph.D. degree specialized in Optics in July 2001 from the Department of Physics, Alabama A&M University, Normal, Alabama. His research interests include thin film, integrated optics, and electro-optic modulators based on NLO materials.

Dr. Jing Ma received his Ph. D. in July 1996 from Chinese Academy of Science, Changchun. He was a research associate in Department of Electrical and Computer Engineering, Northwestern University, Evanston, Illinois. His research in Northwestern University were photonic devices, integration and electro-optical devices based on

nonlinear organic materials. He is currently working in OptoNet, Inc. and his research interest is integrated photonic chip and packaging.

Dr. Bo Liu received his Ph.D. from Institute of Physics, Chinese Academy of Sciences, Beijing. His research interests include nonlinear optics, laser dynamic behavior, quantum optics, and integrated optics.

Dr. Guoyang Xu received his Ph.D. degree in July 1999 from Chinese Academy of Science, Beijing. He is currently a research associate in Department of Electrical and Computer Engineering, Northwestern University, Evanston, Illinois. His current research interests are photonic devices and integration and electro-optical devices based on nonlinear organic materials.

Department of Chemistry, Northwestern University

Prof. Tobin J. Marks received his Ph.D. degree from MIT in 1970. His research interest is in the areas of organometallics, photonics, MOCVD, and molecular electronics.

Dr. Milko E. van der Boom received his Ph.D. degree in organic chemistry in 1999 from the Weizmann Institute of Science, Rehovot, Israel. His current interests include the development of organic nonlinear materials for opto-eleotronic devices.

Hu Kang received his BS degree in Chemistry in 1997 from Tsinghua University, his MS degree in 2000 from Chinese Academy of Sciences, and now is a PhD candidate in Chemistry Department of Northwestern University. His research interests include organic electro-optic materials.

Dr. Peiwang Zhu received his Ph.D. in Applied Chemistry in 1996 from Beijing Institute of Technology. His current interests include organic electro-optical materials, supermolecular self-assembly etc.

Dr. Antonio Facchetti received his PhD degree in Chemistry from University of Milano-Bicocca, Milano in 1997. His main research interests relate to the design, synthesis, and characterization of novel organic chromophores exhibiting large EO response and TPA efficiency for electrooptic modulators and optical switches. Dr. Facchetti is a Research Assistant Professor at Northwestern University and has more than 60 research articles and holds 5 patents.

Dr. Hua Jiang received his Ph.D. degree from University of North Carolina at Chapel Hill. His research interest includes the development of nonlinear organic materials for opto-eleotronic devices.

(8) Appendixes

Appendix A. Introduction

The formation of functional nanoscale multimolecular organizates and the efficient translation of molecular properties into macroscopic observable responses are topics of great current interest. A high level of structural control at nanoscale dimensions is a necessary requirement to exert full control over numerous materials properties (such as optoelectronic etc.). Many factors at the molecular level (e.g., molecular architecture and electronic structure, reactivity, electrostatics, hydrogen bonding, van der Waals interactions, etc.) play an essential role in the design and build-up of structures with elaborate architectural complexity. Crystal engineering, Langmuir-Blodgett (LB) deposition, as well as SA and self-organization, are only a few contemporary examples of many rational approaches to amplifying molecular properties and inducing order and intermolecular communication in condensed molecular matter. In this regard, the formation of device-quality photonic molecular materials represents one promising direction in the scientific quest to gain greater temporal and spacial control over the propagation of light waves in the condensed state. Molecular electro-optic materials offer a particular synthetic challenge since organizing large hyperpolarizability (hence dipolar) building blocks into *acentric microstructures* doubtless incurs large thermodynamic challenges. Nevertheless, substantial progress has been made using electric field processing of glassy polymers, Langmuir-Blodgett film growth, and the self-assembly of covalently interconnected superlattices. In addition to fundamental scientific motivation, the successful formation of high response molecular assemblies with acceptable robustness, transparency, and processing characteristics could lead to novel low switching voltage/large bandwidth electro-optic (EO) light modulators and related devices, promising greatly increased rates of information transmission by enhancing speed, capacity, and bandwidth for optical data networking and telecommunications.

For the above reasons, development of efficient synthetic approaches to the growth and modification of structurally elaborate photonically/electronically functional superlattices with excellent optical, thermal, and chemical properties is of particular scientific interest and potential utility. Among the aforementioned, layer-by-layer siloxane-based SA approaches offer lots of advantages: i) SASs offer far higher EO coefficients and lower dielectric constants than established inorganic materials (e.g., $LiNbO_3$); ii) The chromophores are covalently linked to the substrates, and the films are closely packed and robust. Molecular orientation is intrinsically acentric, and post-deposition processing steps such as poling are not necessary; iii) Chromophore orientation is locked into place with strong covalent bonds, hence the microstructural orientation is very stable; iv) Precise control of film refractive index can be achieved at the sub-wavelength molecular level; v) Absorption bands can be tuned by implanting various building blocks; vi) Large area films can be easily prepared; vii) Chromophore arrays can be fabricated on silicon or a variety of related substrates, allowing ready device integration and therefore significantly reduced device design complexity.

EO modulator is one the key active components in the optical fiber communications system. Organic materials have several advantages (lower dispersion, higher modulation frequency, and lower power of operation) compared with inorganic materials for application in EO devices.

The fabrication and characterization of EO modulators based on novel organic electro-optic materials composed of self-assembled superlattices will be discussed. The SAS structures are intrinsically acentric and exhibit large second harmonic generation and electro-optic responses. This approach using SAS electro-optic materials has advantages such as not requiring poling for creating nonlinearity in the films and efficient film growth on a variety of substrates over large areas. SAS thin films demonstrate long-term stable EO coefficient, and photo-stability at communications wavelengths.

Appendix B. Device Development

Device design, fabrication, test, and materials characterization will be discussed in this section.

B.1. Device Design

Waveguide, optical mode, metal loss, and phase matching, factor critical to high speed application, will be discussed in this subsection.

B.1.1. Ridge waveguide and metal loss

An efficient numerical method for calculating transverse electric (TE) and transverse magnetic (TM) modal properties has been developed and used for the characterization of planar waveguides with loss parameters. Ridge waveguide structure can be evaluated by using the effective index method to incorporate second dimension, and the results were in good agreement with those yielded from sophisticated BPM methods.

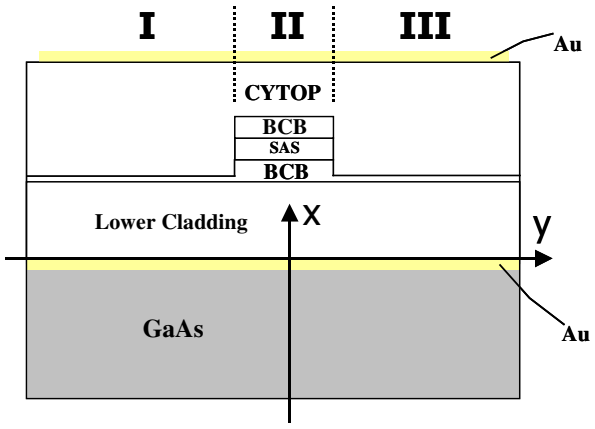

Figure B-1. Cross-section of a waveguide EO modulator.

The cross-section of a typical ridge waveguide is shown in **Figure B-1**, with the bottom electrode located under the lower cladding layer, and the top electrode above the top cladding layer.

The optical modes propagating in the waveguide may be calculated by the beam propagation method (BPM). As a good estimation, in order to find the single mode condition for the ridge waveguide, the ridge waveguide is divided into a central region (region **II**) and two lateral regions (regions **I** and **III**). For each of the three regions, we used an approach that treats the region as a multilayer planar waveguide, and applied transfer matrices that connect

adjacent layers. Effective TE (or TM) mode refractive indices may be obtained for each region. The resultant effective indices for the three regions are used as TM (or TE) refractive index parameters of a symmetric three-layer waveguide having guiding layer thickness t_g. The thickness of the cladding layers was chosen to let the metal loss induced by the electrodes be lower than 0.5 dB/cm. **Figure B-2** shows the bottom metal loss versus the core layer thickness of an EO modulator with 1.4 microns top cladding layer of CYTOP.

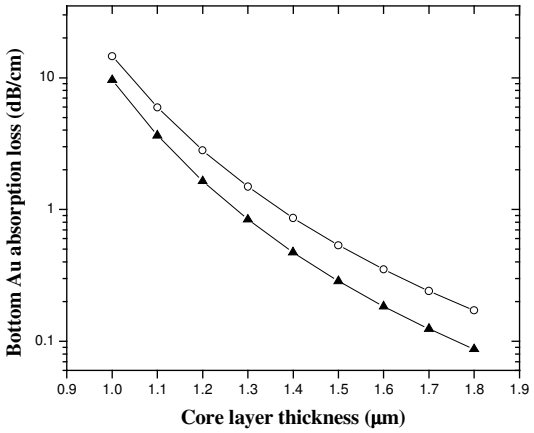

Figure B-2. Bottom metal absorption loss vs. waveguide core layer thickness. Hollow circle, solid triangle correspond to 2.5 μm, 2.7 μm SiO_2 bottom cladding layers. CYTOP is 1.4 μm thick.

B.1.2. Phase matching

Since the refractive indices of polymer materials have much less dispersion with respect to the change of the wavelength than inorganic materials, it is expected that EO modulators based on polymers will have high radio frequency (RF) bandwidth. For high-speed EO modulation application, the mismatch between optical and radio frequency (RF) waves is a factor needed to be minimized. The radio frequency (RF) bandwidth is related to the velocity mismatch between the optical and RF waves and the RF electrode loss. For low-loss materials, the parameters $n_{eff\text{-}opt}$ (effective optical wave refractive index) and $n_{eff\text{-}rf}$ (effective RF wave refractive index) are required for evaluation of f_{3dB}, the RF bandwidth of the electro-optic modulator, which is given by $f_{3dB} = \frac{1.4c}{\pi L(n_{eff-opt} - n_{eff-rf})}$, where L is the length of the electro-optic modulator and c the speed of light in vacuum. We assume that the electrode loss α is negligible here. The index $n_{eff\text{-}opt}$ is estimated using a ridge waveguide configuration as discussed in the previous section and a typical result is shown in **Figure B-3(a)**. The RF effective refractive index $n_{eff\text{-}rf}$ is given by $n_{eff-rf} = \sqrt{\frac{C}{C_0}}$, where C is the capacitance of the structure, as shown in **Figure B-1**, with known dielectric constants for the materials used for a unit length segment of the waveguide, and C_0 is the capacitance while the materials are replaced by air for the same unit length segment. **Figure B-3(b)** shows one of the typical simulation results for the external electric field distribution with the ridge waveguide structure.

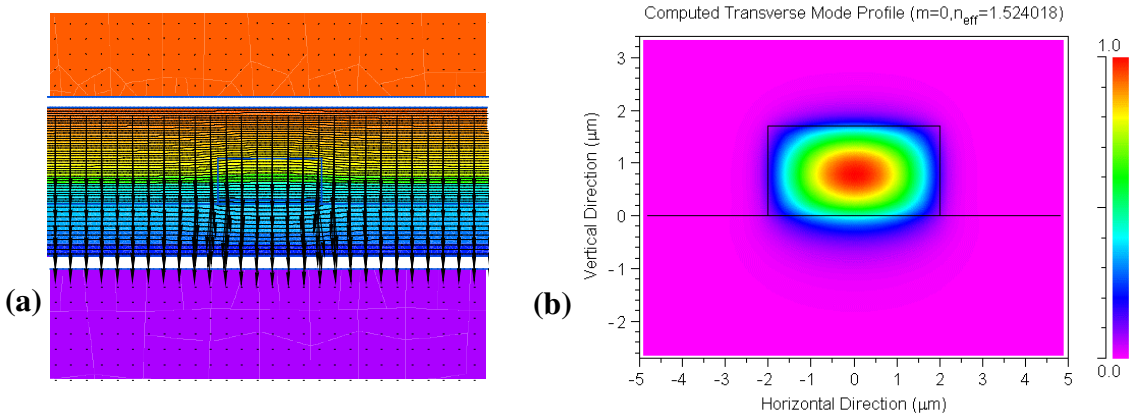

Figure B-3. One of the simulation results. **(a)** The external electric field distribution of the current EO modulator, and **(b)** the optical mode distribution of the EO modulator.

Another factor needed to be addressed for high-speed EO modulation is the characteristic impedance Z, linked with the capacitances by $Z = \frac{1}{c\sqrt{CC_0}}$. For organic materials, it is easier than inorganic materials to match characteristic impedance with the 50Ω transmission line impedance and minimize simultaneously the mismatch between optical and RF waves to achieve high bandwidth since organic materials have low dielectric constants and they are readily processable to make EO active ridge type waveguide by themselves. In one of the simulation samples based on SAS thin layers, the effective optic refractive index $n_{eff\text{-}opt}$ is found to be 1.524 at a wavelength of 1.064 μm. The capacitance of the sample C is 109.2 pF. When the materials are replaced by air, the capacitance C_0 of the virtual sample is 43.04 pF, and the effective RF refractive index $n_{eff\text{-}rf}$ is 1.593. The characteristic impedance Z is 48.6 Ω, which is quite close to the 50Ω transmission line impedance. The difference between $n_{eff\text{-}opt}$ and $n_{eff\text{-}rf}$ is about 0.07, and therefore the mismatch is not a negative factor in achieving a bandwidth of 40 GHz for a waveguide EO modulator based on SAS materials and the above ridge structure.

B.2. Device fabrication and characterization

The first three subsections discuss EO modulators based on SAS thin films grown by three- and two- step processes and their characterization. The following two subsections are on the EO modulators fabricated using EO active thin films by the vapor phase deposition methods. The waveguide EO modulators are fabricated using a multistep process including e-beam deposition, plasma-enhanced chemical vapor deposition, photolithography, and reactive ion etching. The last subsection shows the materials characterization by direct EO coefficient measurement.

B.2.1. EO modulators based on three-step grown SAS thin films

The first self-assembled superlattice (SAS) based electro-optic (EO) modulator and relevant switching voltage measurements were based on SAS thin films fabricated by three-step process.

The waveguide configuration shown schematically in **Figure B-4** has a four-layer stack structure. The commercially available polymer Cytop™ (a fluorinated polyether) is used for the upper cladding layer, and SiO_2 is used as the lower cladding layer. In this work, we used a 40 layer SAS combined with the polymer Cyclotene™ 3022-35 (poly bisbenzocyclobutane or BCB) as the guiding layer. We have measured the thickness of 40 layer SAS to be ~150nm. All polymer waveguides with Cytop/Cyclotene/Cytop structure demonstrated good transparencies (0.5 dB/cm) from 350nm to 1650nm wavelength ranges. The refractive index of Cyclotene™ 3022-35 (n=1.56 at wavelength of 1064 nm) is very close to that of the SAS, and the refractive index of Cytop™ is 1.34 at a wavelength of 1064 nm. SAS were grown by molecular self-assembly. Cyclotene™ and Cytop™ layers were spin-coated onto the SAS layer. The channel waveguide patterns were defined by conventional photolithography, and reactive ion etching (RIE) procedures were carried out to form a ridge waveguide structure.

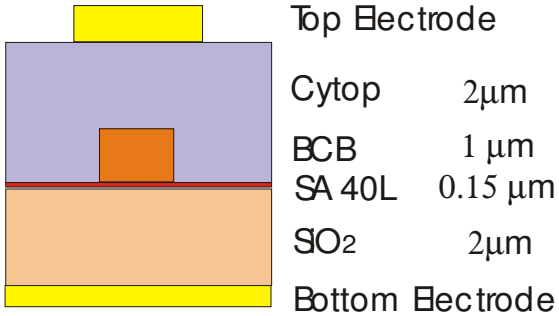

Figure B-4. Modulator device structure

The electro-optic response of the waveguide was measured using the method described in the next section. **Figure B-5** shows the typical EO response of the modulator (5 mm long) measured from the oscilloscope traces. The upper and lower traces in the figure represent the applied electrical signal and the modulator output waveform, respectively. The half-wave voltage-length product, $V_\pi \cdot L$ is determined to be 175 V·cm. From the measured data, the EO coefficient of the SAS material is estimated to be 21.8 pm/V.

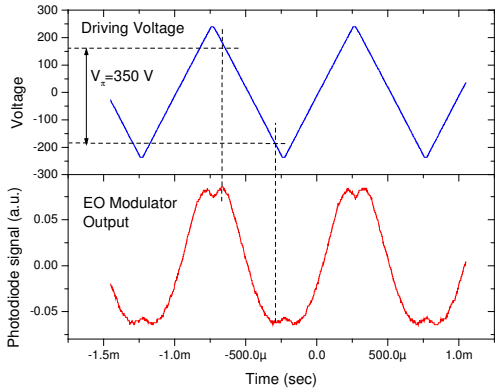

Figure B-5. Switching voltage measurements of a self-assembled EO modulator.

B.2.2. EO modulators based on two-step grown SAS thin films

A new, expeditious two-step process has been developed and used for the growth of SAS films. Prototype modulators with different structures have been fabricated and tested based on the expeditious two-step process. With this process the SAS film can be grown at a rate of about 40 minutes per bilayer (alternating chromophore and capping layer), and it is at least one order of magnitude more rapid than the three-step deposition method. The automation of the two-step process has been demonstrated and yielded high quality SAS thin films on different substrates. **Figure B-6** shows the design structure, and SEM images of the cross-section of an SAS-based waveguide EO modulator fabricated on a GaAs substrate.

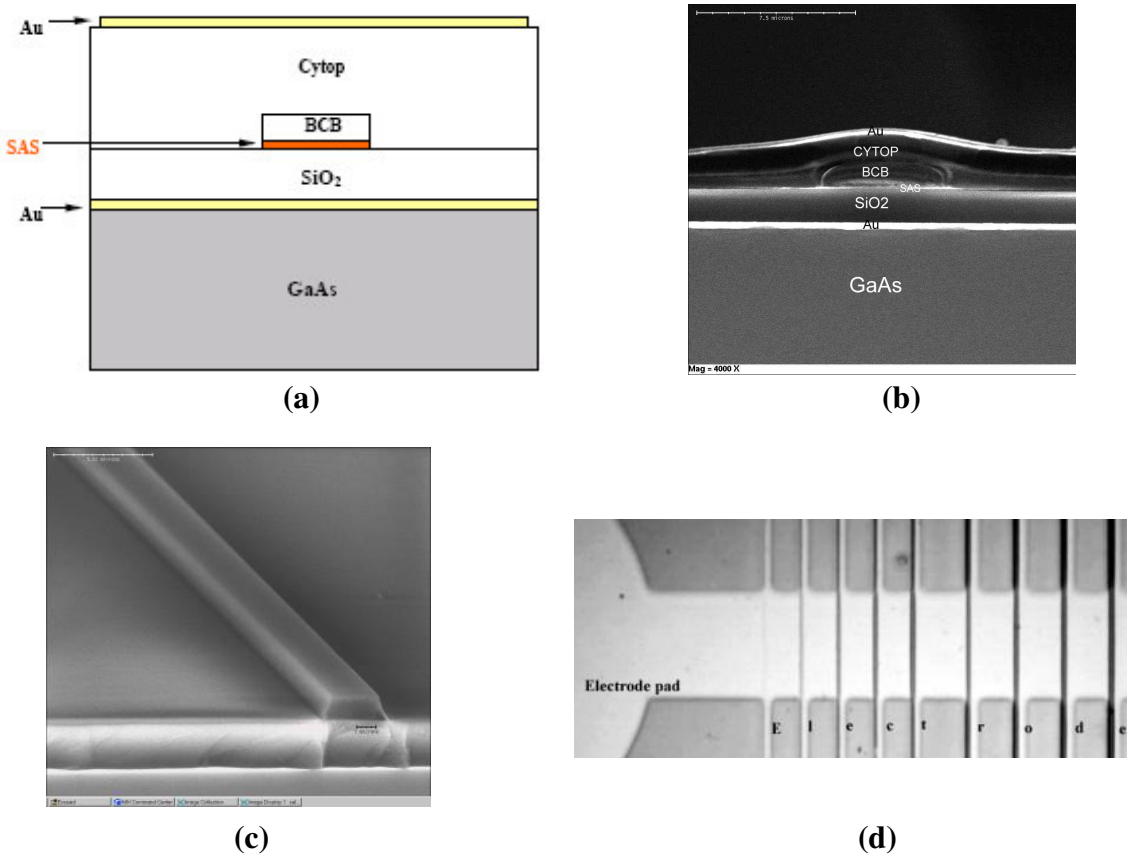

Figure B-6. **(a)** Design structure, and SEM images of **(b)** cross-section, **(c)** ridge waveguide before top cladding spin-coated, and **(d)** top view of electrodes.

The lower Au electrode layer was deposited using a standard E-beam evaporation process. An SiO_2 layer was then deposited by the PECVD method. The EO-active SAS layers were then grown on the SiO_2 layer, and were next covered with a layer of robust, electronic grade polymer BCB. The BCB layer functions as part of the guiding core since it has a good refractive index match with the SAS materials. Next, a low refractive index CYTOP polymer was spin-coated on top of the BCB layer. Both CYTOP and BCB exhibit good transparency over a wide wavelength range from the ultraviolet to infrared and are commercially available. The spin coating conditions were adjusted for a Cytop layer having a thickness of 1.8 μm, and a BCB layer having a thickness of 1.5 μm. In order to form

uniform films, each layer was baked in a conventional oven with nitrogen gas flow after spin coating. Ridge waveguide patterns were next fabricated by etching the BCB to the SiO_2 surface using RIE. Another layer of CYTOP was spin-coated on the ridge structure to form a buried waveguide and to reduce the upper metal contact loss of the optical modes of the waveguides. Finally, the top gold electrode was deposited by using E-beam evaporation and lift-off methods.

We have measured waveguide loss based on the cut-back method (**Figure B-7**). A controlled sample followed same fabrication process as that of the actual EO modulators was used for the measurement. Waveguides were cleaved at different lengths and the intensity of the transmitted light was measured using IR power meter. For the special case of two different lengths by cutting the sample once, the loss, in unit dB/cm, is given by

$$\text{Loss} = 10*\text{Log}_{10}\,[P_1/P_2]/[Z_2-Z_1],$$

where P_1 is the power at the output side of original waveguide, P_2 the power at the output side of the cut-back waveguide, Z_1 the length of the original waveguide, Z_2 the length of the cut-back waveguide.

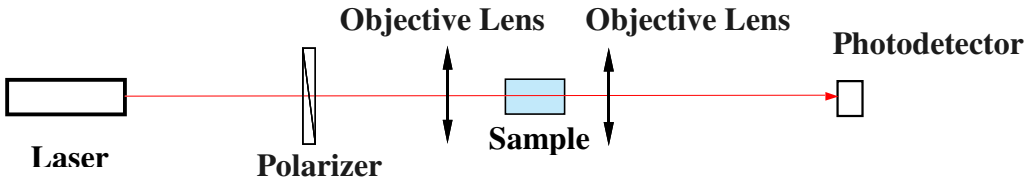

Figure B-7. Schematic of loss measurement of waveguides.

We have also used the top-view method to estimate the loss in waveguides. This method is based on the assumption that the decay of scattered light intensity observed from the top of the waveguide represents the attenuation of the optical mode propagating along the length of the propagating streak. The intensity of the trail of the top scattering light can be easily detected by looking at the surface of the waveguide with a CCD camera.

The EO response of the waveguides was measured by end firing a laser beam from a diode pumped Nd:YAG laser, and it was coupled in and out of the channel waveguide using a pair of microscope objectives (**Figure B-8**). The device was operated by launching both transverse electric and transverse magnetic modes into the waveguide. For recombining the output polarizations, the output light passed through a polarizer oriented at 45° and normal to the direction of the polarizer at the input. The light signal was finally coupled to a photodetector, and was monitored by an oscilloscope. **Figure B-9** shows a typical EO response of the modulator measured from the oscilloscope traces.

The upper and lower traces in **Figure B-9** represent the modulator output wave form and the applied electrical signal, respectively. The half-wave voltage is evaluated to be at the

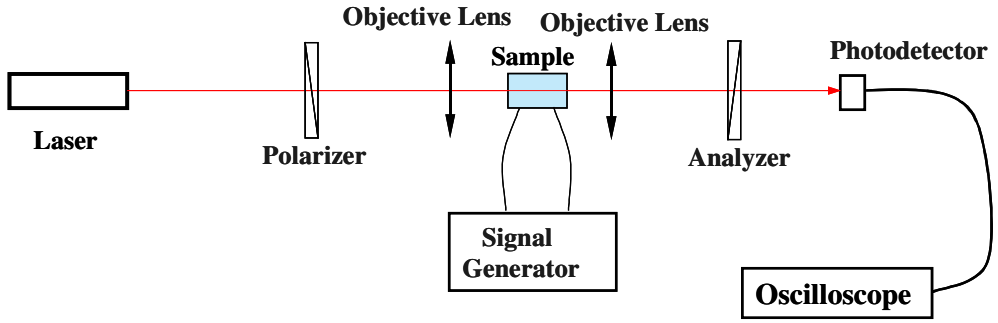

Figure B-8. Schematic of EO response measurement of an SAS-based modulator.

hundred volt level. The effective EO coefficient r is related to the half-wave voltage V_π by $r = \frac{\lambda d}{n_{eff-opt}^{3} V_\pi L \Gamma}$, where λ is the wavelength of the optical wave, d the distance between the lower and the upper electrodes, $n_{eff\text{-}opt}$ the effective optical refractive index, L the length of the electro-optic interaction region, and Γ the overlap integral factor of the optical and the external electric fields, is given by $\Gamma = \frac{d}{V} \frac{\iint E_e |E_o|^2 dxdy}{\iint |E_o|^2 dxdy}$, where the E_e and E_o are the amplitudes of optical field, and external electric field under an applied voltage of V, respectively. The EO coefficient is thus estimated to be on the order of tens of pm/V.

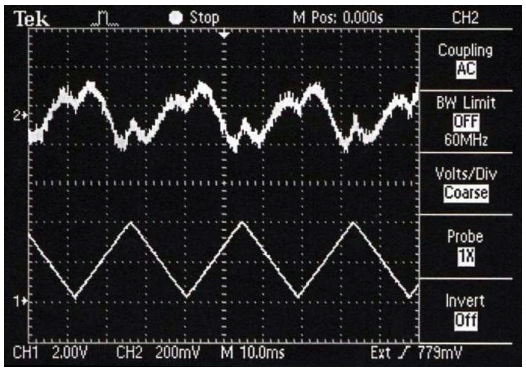

Figure B-9. EO response of an SAS-based modulator monitored by oscilloscope traces. The upper trace is the modulator output wave form, and the lower trace is the applied electrical signal.

B.2.3. EO Modulators based on symmetric waveguide structure

In order to achieve high overlap integral factor Γ for EO modulator and hence reduce driving voltage, symmetric waveguide EO modulator structure has been designed, fabricated, and tested. There will be a factor of 4 improvement of this parameter if the thin film with same thickness was sandwiched between two matching-index polymeric material layers instead of being put on the edge of the ridge waveguide structure.

Figure B-10 shows the design structure and an SEM image of the cross-section of an SAS-based waveguide EO modulator fabricated on a GaAs substrate. The expeditious two-step process has been used for the growth of SAS films. The lower Au electrode layer was

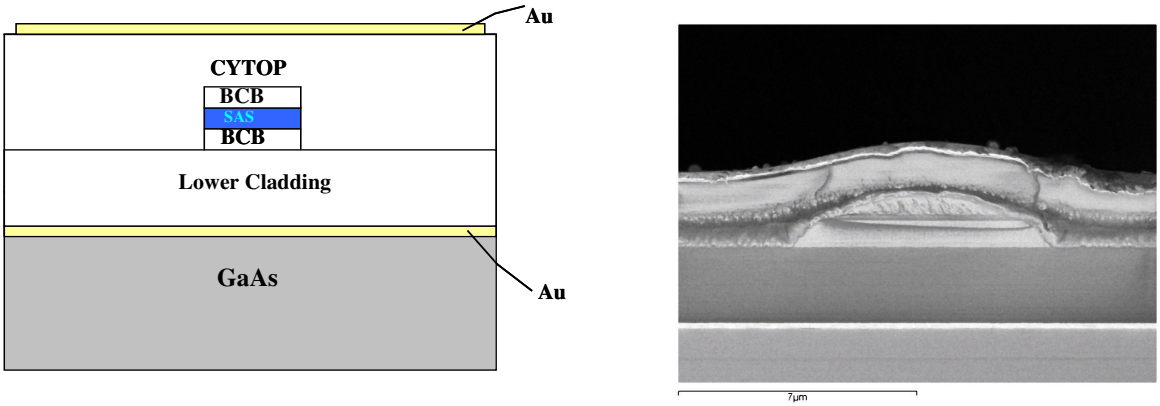

Figure B-10. (a) Design structure, and (b) an SEM image of the cross section of one EO modulator.

deposited using a standard E-beam evaporation process. An SiO_2 layer was then deposited by the PECVD method. A thin BCB layer was then spin-coated and fully cured. The EO-active SAS layers were then grown on the BCB layer, and were next covered with another layer of polymer BCB. The BCB layers function as part of the guiding core since they have good refractive index match with the SAS materials. Next, a low refractive index CYTOP polymer was spin-coated on top of the BCB layer. Ridge waveguide patterns were next fabricated by etching the BCB to the SiO_2 surface using RIE. Another layer of CYTOP was spin-coated on the ridge structure to form a buried waveguide and to reduce the upper metal contact loss of the optical modes of the waveguides. Finally, the top gold electrode was deposited by using E-beam evaporation and lift-off methods.

Figure B-11 shows one typical EO response of the modulator measured from the oscilloscope traces. The half-wave voltage is evaluated to be at the hundred volt level, and the EO coefficient is thus estimated to be on the order of tens of pm/V. At room temperature, the modulation characteristics of the devices exhibit negligible relaxation over a period of several months. Experiments show that the SAS has good thermal stability during the fabrication process involving multiplayer polymer curing, and e-beam deposition.

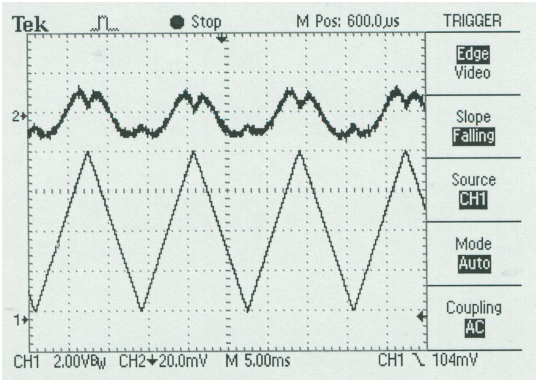

Figure B-11. EO response of an SAS-based symmetric waveguide modulator monitored by oscilloscope traces. The upper trace is the modulator output wave form, and the lower trace is the applied electrical signal.

The next two sections discuss two kinds of vapor phase deposited EO active thin films, which have advantages of fast growth, high optical refractive index, and achievement of EO effect without external electric field poling. Prototype waveguide EO modulators have been fabricated using them as guiding layers with cladding layers having appropriate refractive indices.

B.2.4. Electro-optic modulator based on novel self-assembled thin film of DTPT from vapor phase deposition

The NLO-active chromophore (5-{4-[2-(4,6-diamino-[1,3,5]triazin-2-yl)-vinyl]-benzylidene}-pyrimidine-2,4,6-trione (**DTPT**) containing H-bond donor and acceptor modules was first designed and synthesized. The SA thin films were grown from the vapor phase of DTPT on treated substrates. As the first step for the growth of self-assembled DTPT thin films, a melamine group template was anchored on substrates with 3-amonopropyltrimethoxysilane functionalization carried out by known procedures. The reaction of 6-chloro-1,3,5-triazine-2,4-diamine with 1-propylamine was first carried out in solution to optimize the functionalization reaction conditions for the substrates (Figure **B-12**). The pyrimidine-2,4,6-trione and 4,6-diamino-1,3,5,-trizine-2-yl substituents form longitudinally directed triple H-bonds between neighboring molecules with only head-tail bonding allowed. Intermolecular longitudinal H-bonding interactions force the chromophore molecules to preferentially align in the desired direction (head-tail, perpendicular to the substrate surface) as thin solid films from the vapor phase (**Figure B-13**). Out-plane non-centrosymmetric microstructures are achieved in the deposited films, and the acentricity is intrinsic. Since H-bonding is far stronger than van der Waals forces, the dipolar orientation has high temporal stability with robust film mechanical and environmental properties.

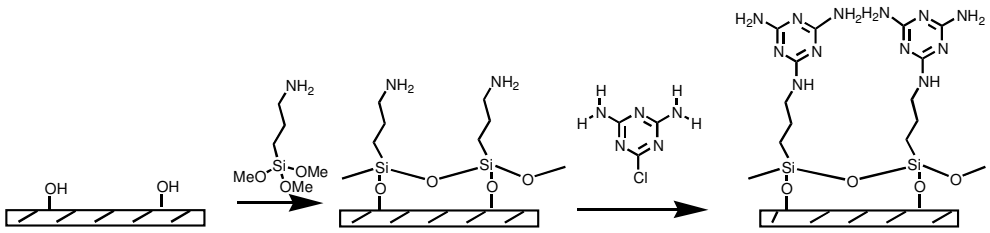

Figure B-12. Functionalization of substrates for self-assembly.

A diffusion-pumped vacuum deposition apparatus (~10^{-8} Torr) was used to grow thin films at a rate of 0.5 - 2 Å/s on substrates with temperature of 100 ^{o}C. This approach is at least one order of magnitude more rapid than the two-step siloxane-based solution deposition methodology. A calibrated quartz crystal microbalance was used to monitor the film growth rate and thickness. The adherent, stable SA thin films exhibit appreciable nonlinear responses, characterized by second harmonic generation (SHG) at a wavelength of 532nm, and a high chromophore surface density. The regularity of the SA thin films has been demonstrated by absorption spectra and SHG responses of samples with different thickness parameters. The SA thin films have been grown on SiO_2, plasma treated polymers, and glass substrates.

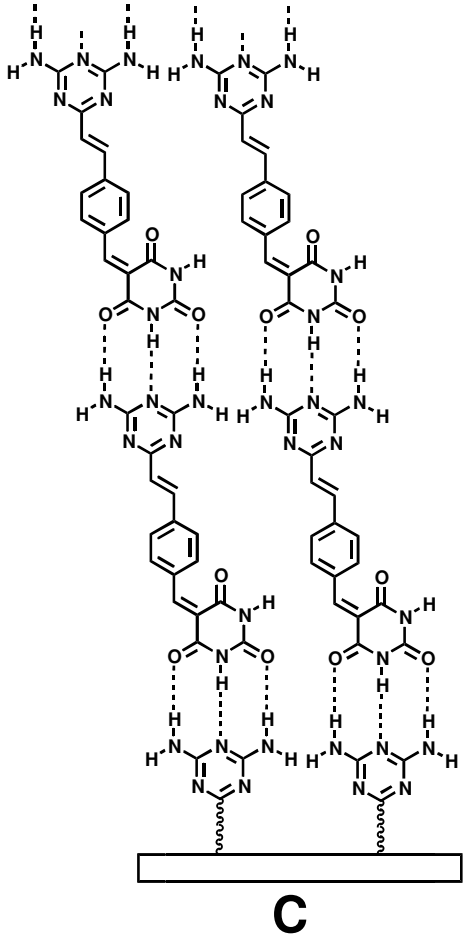

Figure B-13. SA of DTPT on functionalized substrate through H-bonds. Out-plane order is achieved.

Electro-optic waveguide modulators fabricated with DTPT have a three-layer stack configuration. The lower Au electrode layer was deposited using a standard E-beam evaporation process. An SiO_2 layer was then deposited by the PECVD method. The EO-active SA layers were then grown on the SiO_2 layer after an anchor layer by vapor phase deposition as described earlier. Since DTPT has a relatively large refractive index (~1.8 at a wavelength of 632.8nm), simulation and experiment showed that 1 micron thick film is sufficient for DTPT to function exclusively as the guiding layer of the waveguide. Next, a low refractive index CYTOP polymer was spin-coated on top of the SA layer. CYTOP exhibits good transparency over a wide wavelength range from the ultraviolet to infrared and is commercially available. The spin coating condition was adjusted for a CYTOP layer having a thickness of 1.8 μm. In order to form uniform film, the layer was baked in a conventional oven with nitrogen gas flow after spin coating. Ridge waveguide patterns were next fabricated by etching back to the SiO_2 surface using RIE. Another layer of CYTOP was spin-coated on the ridge structure to form a buried waveguide and to reduce the upper metal contact loss of the optical modes of the waveguides. The total thickness of the upper CYTOP

cladding layer is about 1.4μm. Finally, the top gold electrode was fabricated by using E-beam evaporation and lift-off methods.

Figure B-14 shows a typical EO response snapshot of the modulator from oscilloscope traces. The effective EO coefficient is thus estimated to be about 0.13 pm/V and is in good agreement with the SHG measurement. Future chemical engineering of materials with higher nonlinear coefficients will make this process promising.

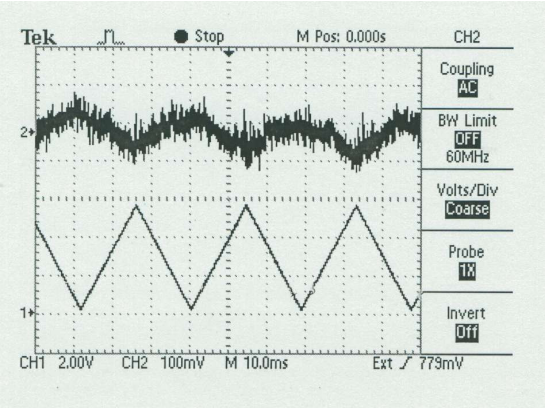

Figure B-14. EO response of a prototype EO modulator based on DTPT thin films. Trace 1 is the applied electrical signal, and trace 2 the response of the EO modulator.

B.2.5. Electro-optic modulator based on novel self-assembled thin film of PEPCOOH from vapor phase deposition

The Structure of PEPCOOH is shown in **Figure B-15**. The compound has been designed and synthesized with the following criteria in mind: (1) π-excessive and π-deficient heteroaromatics as key donor (D) and acceptor (A) NLO core building-blocks,

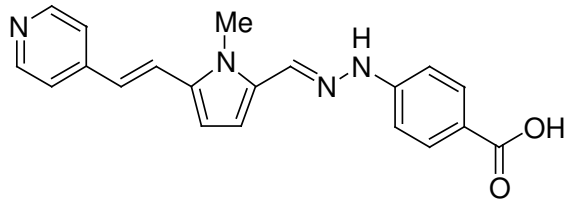

Figure B-15. The chemical structure of PEPCOOH.

(2) presence of H-bond donor (DH) and H-bond acceptor (AH) groups to enforce supramolecular alignment upon sublimation, (3) decoupling between D-A (optical) and DH-AH (assembling) actions through proper molecular design, and (4) stabilization of the NLO chromophore by the presence of groups/atoms that inhibit singlet oxygen-promoted decompositions.

Thermal data show that the present chromophore is thermally very stable. More importantly, TGA data indicate that vacuum-deposited film can be prepared without concomitant chromophore decomposition.

PEPCOOH films can be fabricated on a variety of substrates (glass, quartz, silicon, GaAs, Au-coated glass) by vacuum-deposition under the following experimental conditions:

deposition rate = 0.2-0.3 Å/s, chamber pressure ~ 10^{-5} Torr, substrate temperature = 25-100°C. Film polar order parallel to the substrate normal has been unambiguously demonstrated by second harmonic generation measurements.

To estimate the electro-optic coefficient of PEPCOOH thin film, electro-optic waveguide modulators have been fabricated with BCB and PEPCOOH as core layers, and therefore have a four-layer stack configuration. The lower Au electrode layer was deposited using a standard E-beam evaporation process. An SiO_2 layer was then deposited by the PECVD method.

A layer of robust, electronic grade polymer BCB was then spin-cast and fully cured. The BCB layer functions as part of the guiding core. The EO-active SA layer were then grown on the BCB layer by vapor phase deposition. Next, a low refractive index CYTOP polymer was spin-coated on top of the PEPCOOH layer for process protection. To form uniform film, the layer was baked in a conventional oven with nitrogen gas flow after spin coating. Ridge waveguide patterns were next fabricated by etching back to the SiO_2 surface using RIE. Another layer of CYTOP was spin-coated on the ridge structure to form a buried waveguide and to reduce the upper metal contact loss of the optical modes of the waveguides. The total thickness of the upper CYTOP cladding layer is about 1.4 μm. Finally, the top gold electrode was fabricated by using E-beam evaporation and lift-off methods.

Figure B-16 shows cross-section of a typical EO modulator, and an EO response snapshot of the device is shown in **Figure B-17**. The EO coefficient is estimated in the order of tens of pm/V.

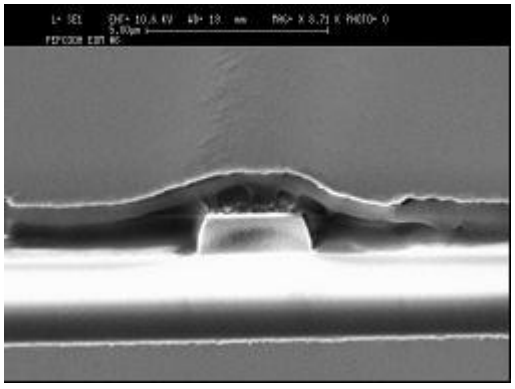

Figure B-16. Cross-section SEM image of a typical ridge waveguide EO modulator based on PEPCOOH.

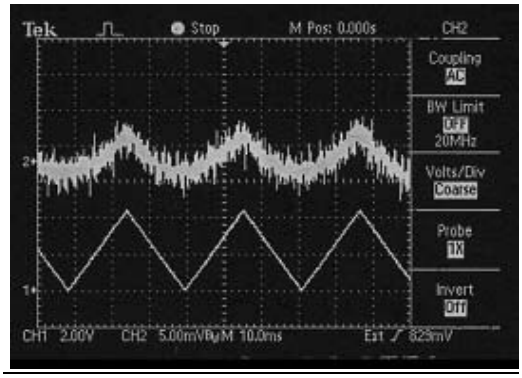

Figure B-17. EO response of a prototype EO modulator based on a PEPCOOH thin film. Trace 1 is the applied electrical signal, and trace 2 the response of the EO modulator.

Deuteration of the hydrogen bonds should lower the absorption of the materials, and is currently under investigation. Future chemical engineering of materials with higher nonlinear coefficients will make this process promising since the growth rate is on the order of ten hours and the thin films are flat enough for good waveguide fabrication.

B.2.6. Direct EO coefficient measurement

In order to quickly evaluate EO coefficients of EO active thin films without waveguide fabrication, we have set up a high sensitivity direct EO coefficient measurement device based on the Teng-Man method. **Figure B-18** shows the schematic of the direct EO coefficient measurement set-up configuration. TCO layer is deposited on substrate glass. The EO thin films were grown on the TCO layer. Gold electrode is deposited on the EO thin films by e-beam evaporation. The alternating current (AC) drive voltage is applied to the EO sample, and the modulated signal is monitored and processed by an oscilloscope and lock-in amplifier. The wavelength ranges are from 632.8 nm to 1550 nm using different laser sources. The sensitivity of the measurement is about 1.0 pm/V under drive voltage of 10V.

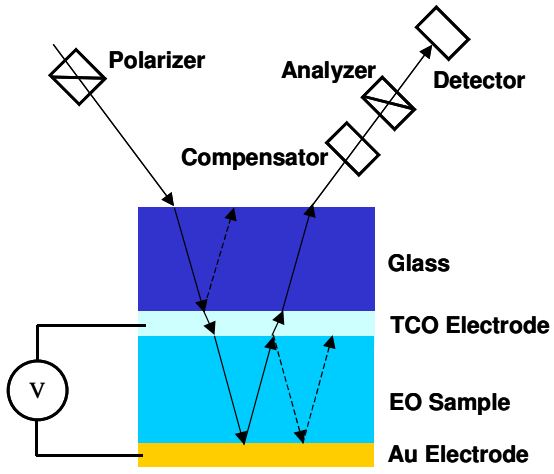

Figure B-18. Teng-Man setup for measurement of thin films' EO coefficients

Figure B-19 shows a calibration measurement result of a $LiNbO_3$ crystal. The Teng-Man measurement method uses the phase sensitivity, with the measurable phase change $\Delta nL = (1/2)n^3 r_{33} EL = n^3 r_{33} V$. From this figure, even with a drive voltage of about 0.3V, we have detectable signal. The minimum phase change that can be measured is about $(\Delta nL)_{Min} = 2.2^3 30(pm/V) * 0.3V \approx 96pm$. If we apply a drive voltage of 10V (the upper limit of signal generator used) to the sample, the minimum EO coefficient we can measure is

$$(r_{33})_{Min} = ((\Delta nL)_{Min} / n^3 V) = (96pm / 2.2^3 * 10V) \approx 1pm/V .$$

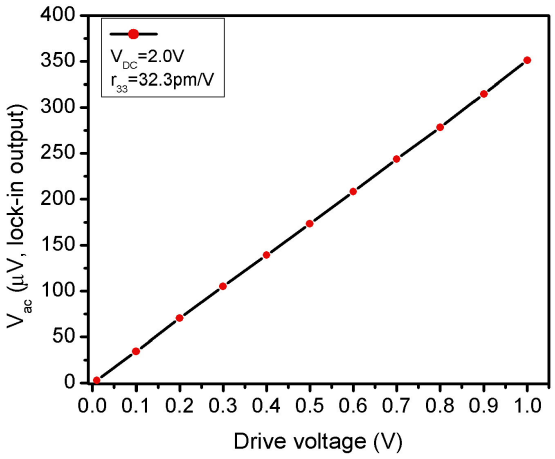

Figure B-19. Teng-Man measurement data for lithium niobate crystal. The evaluated value of 32.3 pm/V for r_{33} is in good agreement with literature values.

Appendix C. Materials Development

C.1. Streamlining the SAS growth process

A new, expeditious siloxane-based layer-by-layer assembly process for the formation of intrinsically polar organic electro-optic thin films has been developed using highly reactive – $SiCl_2I$-functionalized, silyl-protected donor-acceptor azo-benzene chromophore derivatives and octachlorotrisiloxane as a deprotecting reagent/interlayer precursor. This all-"wet-chemical" two-step process can be efficiently implemented in a vertical dipping procedure to yield polar films consisting of 80 alternating chromophore and capping layers. The procedure is shown in **Figure C-1**. The nanoscale bilayers (chromophore +

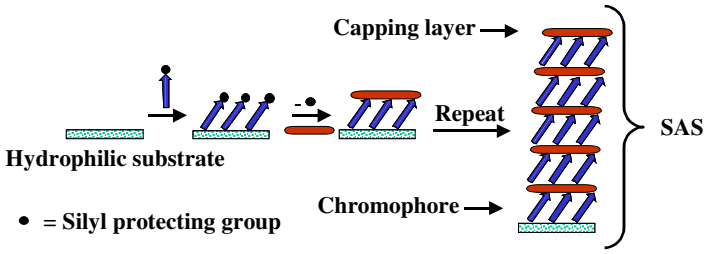

Figure C-1. Schematic representation of the new two-step layer-by-layer self-assembly of self-assembled superlattices. The procedure can be performed using a single reaction vessel and standard cannula techniques, or by immersion of the substrates in reagent and washing solutions within a nitrogen-filled glovebag.

polysiloxane layer ≈ 3.26 nm thick) can be grown in ~ 40 min. – at least one order of magnitude more rapidly than conventional siloxane-based solution deposition methodologies. Chromophore monolayer deposition from solution reaches completion in ~15 min. at 55 °C (**Figure C-2**). The adherent, structurally regular assemblies exhibit appreciable electro-optic responses ($\chi^{(2)}$ ~180 pm/V and r_{33} ~65 pm/V at 1064 nm), high chromophore

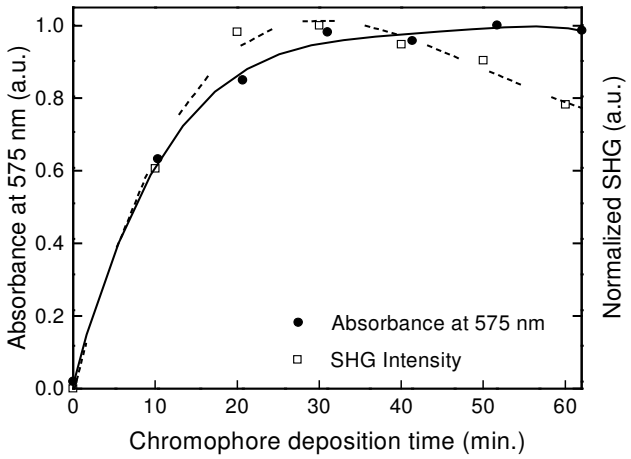

Figure C-2. Optical spectroscopic data and second-harmonic generation (SHG) response measurements as a function of reaction/deposition time for the formation of a chromophoric monolayer from THF solution (8.0 mM chromophore concentration, 50 °C) on a float glass substrate.

surface densities (~40 $Å^2$/chromophore), and have been characterized by a full complement of physicochemical techniques: optical spectroscopy (UV-vis), aqueous contact-angle (CA) measurements, specular X-ray reflectivity (XRR), atomic force microscopy (AFM), and angle-dependent polarized second harmonic generation (SHG). All of these measurements show regular SAS growth up to 80 layers (e.g., **Figures C-3**, **C-4**).

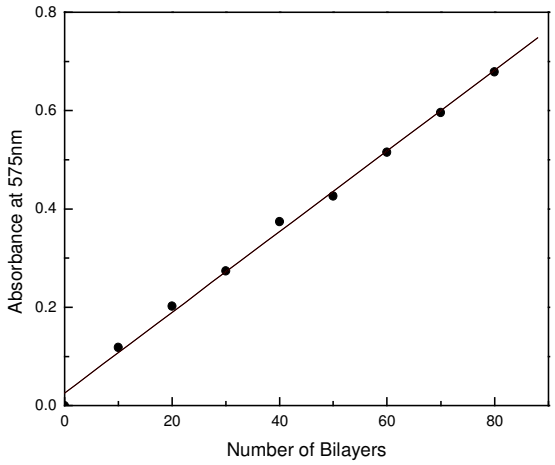

Figure C-3. Optical absorption spectra of SAS films at 575 nm as a function of the number of chromophore-based bilayers. The solid line is the fit by linear regression.

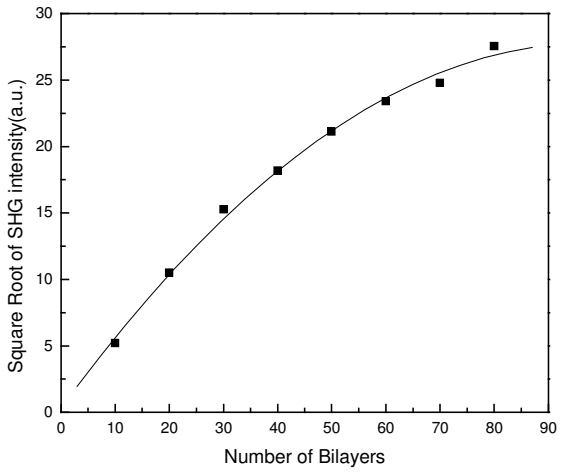

Figure C-4. Absorption corrected square-root of SAS 532 nm SHG response ($I_{corrected}^{2\omega}$) as a function of the number of bilayers.

C.2. SAS refractive index tuning

The refractive indices of self-assembled organic electro-optic superlattices can be tuned by intercalating high-Z optically transparent group 13 metal oxide sheets into the structures during the self-assembly process (**Figure C-5**). Microstructurally regular acentricity and sizable electro-optic responses are retained in this straightforward synthetic procedure. This "one-pot" all wet-chemistry approach involves: (i) layer-by-layer covalent self-assembly of intrinsically acentric multilayers of high-hyperpolarizability chromophores on inorganic oxide substrates, (ii) protecting group cleavage to generate a large density of reactive surface hydroxyl sites, (iii) self-limiting capping of each chromophore layer with octachlorotrisiloxane, (iv) deposition of metal oxide sheets derived from THF solutions of $Ga(O^iC_3H_7)_3$ or $In(O^iC_3H_7)_3$, and (v) covalent capping of the resulting superlattices. **Figure C-6** shows the degree to which the SAS index of refraction can be tuned—unprecedented for an organic electro-optic material.

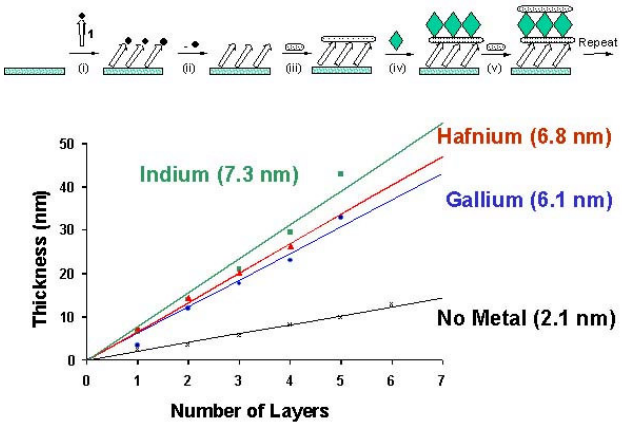

Figure C-5. Scheme for the introduction of high-Z metal oxide nanolayers into SAS structures. The regular of X-ray determined film thickness as a function of the number of layers is shown.

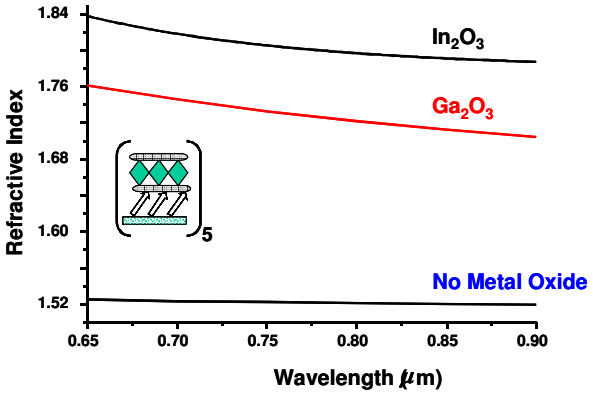

Figure C-6. Index of refraction data for metal oxide intercalated SAS films.

C.3. Introduction of high-response chromophores into SAS structures

A broadly applicable approach to the formation of self-assembled organic electro-optic materials for high-speed switching is reported. This two-step "one-pot" all wet-chemical method involves: (i) layer-by-layer covalent self-assembly of intrinsically acentric monolayers of a new high-hyperpolarizability donor-acceptor chromophore (**Figure C-7**) on inorganic oxide substrates, and (ii) *in-situ* chromophore deprotection concurrent with

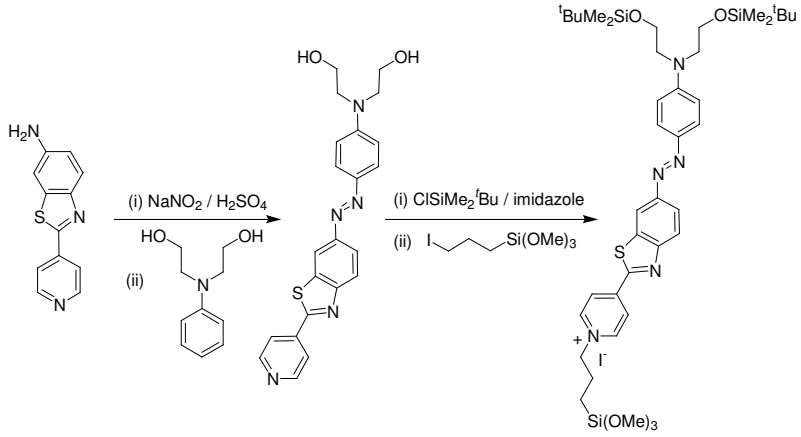

Figure C-7. Synthesis of new thiophene-based chromophore and the corresponding high-hyperpolarizability *n*-propyl-3-trimethoxysilane pyridinium iodide salt for SAS construction.

self-limiting "capping"/planarization of each chromophore layer with octachlorotri-siloxane. The functional superlattices exhibit very large second-order responses, $\chi^{(2)} \approx 370$ pm/V, and a large macroscopic electro-optic coefficient, $r_{33} \approx 120$ pm/V, is estimated at $\lambda_0 = 1064$ nm.

A novel thiophene-containing chromophore (NU2) was also developed (**Figure C-8**). This chromophore show great SHG response. Self-assembled monolayer was obtained via the first generation methodology, which shows the $\chi^{(2)}$ value be around 570 pm/V, and a large macroscopic electro-optic coefficient, $r_{33} \approx 190$ pm/V, is estimated at $\lambda_0 = 1064$ nm.

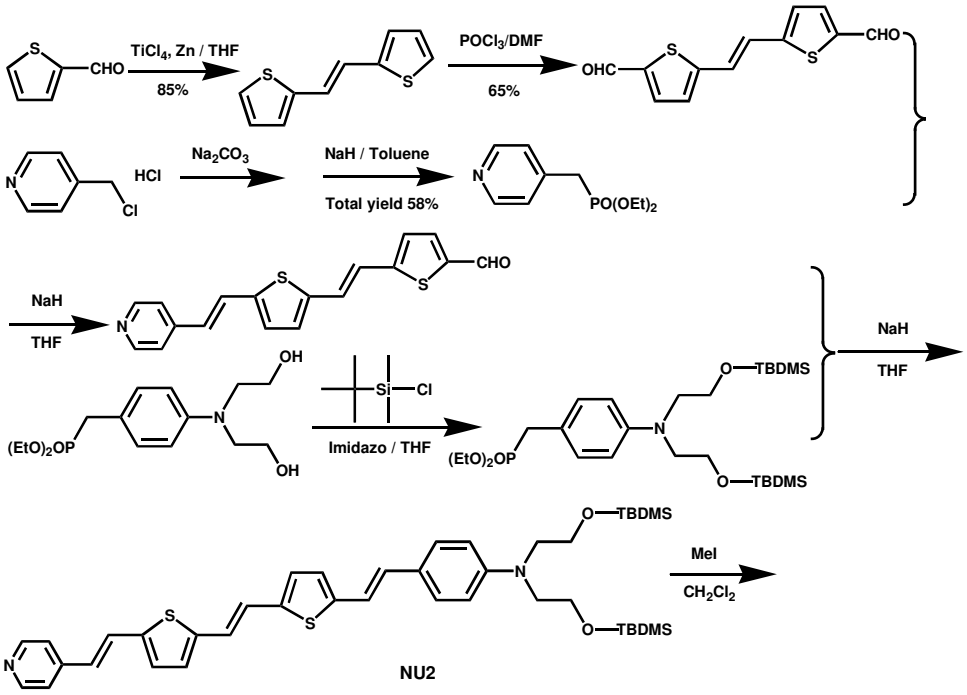

Figure C-8. Synthesis of new thiophene-containing chromophore (NU2).

C.4. Stability of SAS against irradiation

Two SAS samples (22 bilayers and 24 bilayers prepared according to the scheme shown in **Figure C-1**) were irradiated to test the stability property. The UV-vis spectra of the irradiated samples show almost the same λ_{max} and the absorption intensities as those before irradiation (**Figure C-9**). SHG measurements show no nonlinearity decay after the irradiation (**Tables 1** and **2**). The nonlinearities increased about 15% (22-bilayers sample), and 4% (24-bilayers sample) respectively. Since SHG data were measured at different time (before and after irradiation), the increase might be due to the error (~ 15%) caused by the system fluctuation. More accurate measurements will be done at the same conditions.

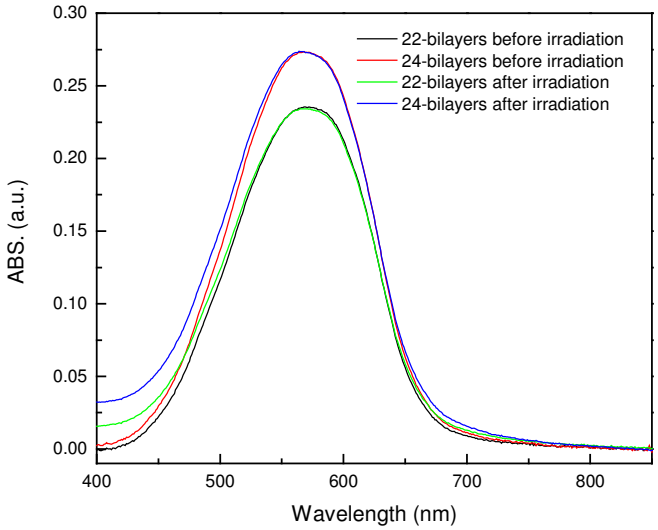

Figure C-9. UV-spectra of SAS before and after irradiation.

Table 1. Comparison of SHG intensities of 22-bilayers sample before and after irradiation

	$I_q^{(2\omega)}$	$I_s^{(2\omega)}$	$(I_s^{(2\omega)}/ I_q^{(2\omega)})^{1/2}$
Before Irradiation	234.93217	2.97894	0.1126
After Irradiation spot1	201.56073	3.28714	0.1277
After Irradiation spot2		3.46013	0.1310
After Irradiation Average			0.1294

Table 2. Comparison of SHG intensities of 24-bilayers sample before and after irradiation

	$I_q^{(2\omega)}$	$I_s^{(2\omega)}$	$(I_s^{(2\omega)}/ I_q^{(2\omega)})^{1/2}$
Before Irradiation	234.93217	3.94764	0.1296
After Irradiation spot1	201.56073	3.59825	0.1336
After Irradiation spot2		3.78371	0.1370
After Irradiation Average			0.1353